coatings

MDPI

Article

New Transparent Flame-Retardant (FR) Coatings Based on Epoxy-Aluminum Hypophosphite Nanocomposites

Fouad Laoutid [1,*], Maryam Jouyandeh [2], Oltea Murariu [1], Henri Vahabi [2], Mohammad Reza Saeb [3], Loic Brison [1], Marius Murariu [1] and Philippe Dubois [1]

[1] Laboratory of Polymeric and Composite Materials, Materia Nova Materials R&D Center & UMONS Innovation Center, 3 Avenue Copernic, 7000 Mons, Belgium
[2] Université de Lorraine, CentraleSupélec, LMOPS, F-57000 Metz, France
[3] Department of Polymer Technology, Faculty of Chemistry, Gdańsk University of Technology, G. Narutowicza 11/12, 80-233 Gdańsk, Poland
* Correspondence: fouad.laoutid@materianova.be; Tel.: +32-65-554978

Abstract: The present study investigated the flame-retardant (FR) effect of transparent epoxy coating containing aluminum hypophosphite (AHP) nanoparticles (NPs) on polylactic acid (PLA) sheets used as a typical model of combustible polymeric material. First, AHP NPs (≤60 nm) were prepared by a specific two-stage wet milling process and deeply analyzed (morphology, thermal/mechanisms of degradation under nitrogen and air). The thermal properties of epoxy–AHP nanocomposites were compared with the pristine epoxy resin. The addition of AHP NPs into epoxy resin accelerated thermal degradation of the coating, thereby increasing the amount of char residue. The application of blank epoxy coating on the surface of PLA plate slightly made PLA more ignitable, without any reduction in the peak of heat release rate (pHRR). The decrease of time to ignition (TTI) was more important in the presence of AHP NPs due to their reactivity toward epoxy resin. Epoxy coating containing 15 wt.% AHP NPs showed the most significant reduction in pHRR as the result of the formation of a homogenous char layer. Further increase of AHP NPs content up to 20 wt.% did not end in any further enhancement, as a consequence of structural cracks observed in the coating that prevent the formation of an effective char. The coated samples remained transparent, promisingly paving the way to appropriate decorative flame-retardant coatings.

Keywords: epoxy nanocomposites; flame-retardant coatings; aluminum hypophosphite; thermal degradation; fire testing

check for updates

Citation: Laoutid, F.; Jouyandeh, M.; Murariu, O.; Vahabi, H.; Saeb, M.R.; Brison, L.; Murariu, M.; Dubois, P. New Transparent Flame-Retardant (FR) Coatings Based on Epoxy-Aluminum Hypophosphite Nanocomposites. *Coatings* **2023**, *13*, 140. https://doi.org/10.3390/coatings13010140

Academic Editor: Mazeyar Parvinzadeh Gashti

Received: 30 November 2022
Revised: 24 December 2022
Accepted: 5 January 2023
Published: 10 January 2023

Copyright: © 2023 by the authors. Licensee MDPI, Basel, Switzerland. This article is an open access article distributed under the terms and conditions of the Creative Commons Attribution (CC BY) license (https://creativecommons.org/licenses/by/4.0/).

1. Introduction

Epoxy resins are high-performance materials presenting acceptable chemical resistance, corrosion resistance and adhesion, making them fit to several applications such as adhesives, coatings, structural laminates and electrical devices [1–3]. However, they suffer from a high fire risk because of their low flame retardant (FR) characteristics [4–6]. For applications requiring high flame retardancy materials, the enhancement of their fire behavior is crucial and a considerable attention has been devoted to the production of FR epoxy composites by using halogen-free additives, i.e., phosphorus–based additives [7–11]. For more information regarding the current trends in production of FR epoxy composites, we recommend a comprehensive review paper published recently, based on the classification of FR additives in terms of phosphorus, non-phosphorus, and their combinations in terms of Flame Retardancy Index (FRI) [12]. They are also privileged due to transparency while keeping their performance [13–15].

Using nanoparticles (NPs) for enhancing the fire retardancy of polymeric materials has been of great interest in the last two decades [16]. Layered silicates (clays) are among the most frequently used NPs owing to promising barrierity resulting from their platelet-like structure, large surface area and high aspect ratio, acceptable costs and the possibility

of chemical surface modification to facilitate their dispersion in different polymers [17]. Even at low loadings (3–5 wt.%), the incorporation of such lamellar NPs solely results in appropriate fire protection of polymers as attested by cone calorimeter testing, but not necessarily in vertical propagation testing. A similar behavior was typically evidenced in the case of PLA (nano)composites, e.g., filled with organoclays, expanded graphite and/or carbon nanotubes [18,19]. This is due to the horizontal configuration of the cone calorimeter test, which avoids the flow of the melt and favors the formation of a protective layer induced by the accumulation of NPs on the surface of the plate-shaped specimens. Enhanced FR properties, as evidenced by vertical tests such UL-94 or limiting oxygen index (LOI), could also be obtained when the NPs are associated with other flame retardants [17–20] or they underwent surface chemical modifications by the grafting of reactive molecules, generally phosphorated ones [21–25]. The use of phosphorus-based FRs at the nanoscale could be an interesting strategy for improving their efficiency and obtaining appropriate mechanical properties while keeping transparency. To date, to the best of the knowledge of the authors of this work, no study has focused on the use of phosphorus-based flame retardant at the nanoscale, and the use of these agents were quite often of micron size. Aluminum hypophosphite (AHP) seems to be an appropriate candidate to succeed in this challenge. AHP was introduced to the market about two decades ago, but it is still actively researched for new applications by industrial laboratories and similarly academic researchers to unravel its FR action mechanisms [26]. Indeed, AHP has demonstrated its effective FR effect in various polymers such as polyethylene terephthalate [27], polyamide [28], PLA [29,30], polystyrene [31], polyurethane [32], and others [33,34], owing to (i) the high phosphorus content (>41%) 29, (ii) low oxidation degree that can promote an effective gas phase FR action, and (iii) the presence of aluminum at high content that is well known to induce synergistic FR effects with phosphorus in the condensed phase [35]. However, AHP is added in different polymers in high percentage (up to 30 wt.%) and presents some fire risk and toxicity, arising from decomposition at relatively low temperature (250–300 °C) and releasing toxic phosphine that may spontaneously ignite in air and even form explosive mixtures with air in extreme cases [28,36,37].

Regarding the FR action of AHP, it is largely agreed that AHP first decomposes with evolution of 1.5 moles of phosphine, which is quickly oxidized in the flame, firstly providing a gas phase inhibition effect [26]. Therefore, the use of AHP is limited to polymers that could be traditionally melt-processed below 250 °C. Calcium hypophosphite (CaHP) is more stable than AHP and can therefore be used at higher temperatures (thermal degradation above 350 °C [38]), but unfortunately it produces less phosphine and consequently, is less efficient as FR additive [26]. FRs based on these products are marketed by Italmatch Chemicals company under the brand name Phoslite®. The fire safety during the production, storage, and use of AHP could be enhanced by its encapsulation [37,39]. Ge et al. [37] prepared microencapsulated AHP (MCAHP) by melamine cyanurate (MCA) that could form a protective layer and thereby enhance AHP fire safety by inhibiting its thermal degradation, decelerating phosphine formation and diluting phosphine by inert MCA decomposition product.

In a previous study [40], we explored a new safe way for using nanosized AHP in FR applications. AHP microparticles were firstly transformed in NPs by wet grinding into ethanol. Under such condition, AHP NPs could be securely stored as a suspension in a suitable solvent prior to be incorporated into wet coatings, without the need for any thermal treatment above 200 °C. The obtained suspension was then incorporated into an epoxy resin at different AHP content. The effect of the incorporation of AHP NPs on the curing behavior and crosslinking degree of epoxy resins has been previously studied. The results highlighted positive effect of the presence of AHP NPs that induced the formation of a denser crosslinked network, through the action of aluminum cation as a reactive Lewis acid element [41]. Herein, we applied epoxy/AHP transparent nanocomposites as a coating onto PLA sheets. The thermal and FR properties of epoxy/AHP nanocomposites are also analyzed prior to be used as a coating on PLA sheets to protect them against fire. PLA

MOST WIEDZY Downloaded from mostwiedzy.pl

sheets were used as typical combustible polymer materials in order to evaluate the potential FR effect of epoxy/AHP NPs coating. The FR properties of PLA coated by epoxy/AHP nanocomposites were evaluated by mass loss cone calorimeter (MLC) tests. Furthermore, the thermal insulating effect of epoxy/AHP nanocomposite coating was monitored by measuring the evolution of the temperature on the exposed and non–exposed surfaces during the combustion.

2. Materials and Methods

2.1. Materials

Epoxy resin and its curing agent were EPIKOTE Resin 828 (viscosity of 12.0–14.0 Pa.s at 25 °C and density of 1.16 g/mL) and EPIKURE F205 (viscosity of 0.5–0.7 Pas at 25 °C and density of 1.04 g/mL), provided by Hexion, Houston, TX, USA.

AHP microparticles were purchased from Hutong Global Co., Ltd. (Tianjin, China). According to supplier the purity of product was higher than 99%, the granulometry of microparticles was about 10 microns, whereas its initial thermal decomposition temperature was $\geq$280 °C (the conditions of thermal analysis not specified). PLA was purchased from NatureWorks (Ingeo 3251D, ≈1.4% D-isomer).

2.2. Preparation of AHP Nanoparticles

AHP microparticles were used for the preparation of AHP NPs by a two–step milling process by SDTech Nano France (Alès, France), in ethanol (technical grade from VWR) using microbeads Netzsch Labstar mill. First, AHP microparticles size was reduced up to 1 μm using grinding balls with a diameter of 1 mm and a grid mesh with the size of 400 μm. During the second step, smaller grinding balls (diameter of 200 μm) and grid mesh (diameter of 100 μm) were used for obtaining AHP NPs with a diameter lower than 60 nm.

2.3. Preparation of Epoxy/AHP Nanocomposites

Epoxy nanocomposites containing 5, 10, 15 and 20 wt.% AHP NPs were separately obtained by mixing AHP/ethanol (9 wt.%) solution and epoxy resin under sonication for 5 min followed by a mechanical stirring at 1500 rpm for 20 min. After complete solvent evaporation in an oven at 45 °C for 24 h, the hardener was added to the so obtained blend at weight ratio of 100:58 (resin/hardener), based on stoichiometric molar proportion with EPIKOTE Resin 828, at ambient temperature and stirred for 3 min.

2.4. Preparation of PLA Coated by Epoxy/AHP Nanocomposites

Neat PLA was dried in vacuum at 60 °C for 4 h before injection molding. Sample dimensions 100 × 100 × 4 mm^3, for MLC test, were obtained using an injection-molding machine, Krauss Maffei KM 50. The plates of pristine PLA were coated with the epoxy mixtures to obtain film layers of pristine epoxy and epoxy-AHP nanocomposites. The prepared epoxy compositions (with/without NPs) were placed on the surface of PLA plates as layers with the thickness of about 100 μm, by a film applicator. Then, the coated films cured at room temperature for 7 days.

2.5. Characterization Methods

2.5.1. Electron Microscopy

Scanning electron microscopy (SEM) and scanning transmission electron microscopy (STEM) analyses were performed using an ultra-high-resolution FE-SEM SU-8020 Hitachi microscope (Hitachi, Tokyo, Japan) equipped with triple detectors. The microscopic observations of AHP microparticles and NPs were accomplished respectively, by SEM (SE mode, at an acceleration voltage of 5 kV) and by STEM (TE mode, at 30 kV). Selected samples of epoxy/AHP nanocomposites were characterized to derive information about their morphology.

MOST WIEDZY Downloaded from mostwiedzy.pl

2.5.2. Thermogravimetric Analysis (TGA)

In order to study the thermal stability of AHP, TGA analysis was performed using a TGA Q50 (TA Instruments, New Castle, DE, USA) by heating the samples (AHP NPs and microparticles) under nitrogen or air, from room temperature (RT) up to max. 800 °C (platinum pans, heating ramp of 20 °C/min, 60 mL/min nitrogen or air flow for sample, and 40 mL/min nitrogen as gas purge for the microbalance of the instrument).

The thermal stabilities of fully cured pristine epoxy resin and its nanocomposites were evaluated on a STA–6000 instrument (Perkin–Elmer, Norwalk, CT, USA) within a temperature range of 25–700 °C under a heating rate of 10 °C/min in N_2 atmosphere with a flow rate of 20 mL/min. For this purpose, about 8 mg of samples were weighed and placed in a ceramic crucible. This analysis was performed in order to evaluate thermal stability of epoxy/AHP nanocomposites.

In TGA, the initial decomposition temperature ($T_{5\%}$, °C) was typically considered as the temperature at which the weight loss is 5 wt.%, and the temperature of the maximum mass loss rate (T_d) was defined as the temperature at which the samples present the maximal mass loss rate. Likewise, $T_{10\%}$, and $T_{50\%}$ were defined, along with the char residues were quantified from TGA thermograms and tabulated.

2.5.3. Fire Testing

Pyrolysis combustion flow calorimetry (PCFC) tests were performed on small quantities (2–4 mg) of epoxy/AHP nanocomposites using fire testing technology (FTT Ltd., East Grinstead, West Sussex, UK) apparatus, according to the ASTM D7309. Samples were first heated at 1 $K.s^{-1}$ up to 750 °C under nitrogen, and the pyrolysis products were directly transferred into a combustor chamber (at 900 °C and under N_2/O_2 80/20 atmosphere), in which they underwent a complete oxidation. Calculation of the heat release rate (HRR) was based on the oxygen consumption according to Huggett's relation (1 kg of consumed oxygen corresponds to 13.1 MJ of released heat) [42].

The fire behavior of PLA and coated PLA plates was evaluated by MLC (from FTT, Ltd., East Grinstead, West Sussex UK), equipped with a thermopile and chimney for heat release assessment, according to the ISO 17554 standard. The 100 × 100 × 4 mm^3 sheets already prepared by injection molding were exposed to a radiant cone (35 $kW.m^{-2}$). For each formulation, at least, two samples were tested. Temperature evolution on exposed and unexposed sides of the plates was monitored using a thermocouple data logger (Pico Technology USB TC-08).

3. Results and Discussion

3.1. Characterization of AHP Nanoparticles

3.1.1. Morphology of AHP NPs

The two-step milling process, performed on AHP microparticles (Figure 1a), enabled successful downsizing and the generation of new NPs with a diameters less than 60 nm, as attested by STEM images (Figure 1b). The preservation of AHP NPs in ethanol prevented their aggregation.

3.1.2. Thermal Analyses

The thermal decomposition behavior of AHP was analyzed by TGA in nitrogen and air atmospheres (TGA data summarized in Table 1). Figure 2 shows the comparative TGA and derivative thermogravimetic (DTG) traces of AHP microparticles and NPs analyzed under nitrogen. It turned out that the thermal degradation of AHP began at about 300 °C, whereas the highest rates of decomposition were seen at 344 °C for NPs and 361 °C for microparticles, differences are mainly ascribed to their morphologies/physical dimensions. In the first step of thermal degradation (noted with (I) in Figure 2), as frequently considered in the literature, a shoulder was seen in the range of temperature of 300–350 °C [43], where AHP decomposed to produce phosphine (PH_3) and aluminum hydrogen phosphate [$Al_2(HPO_4)_3$]. At higher temperatures (above 400 °C, step II), a second weight loss was

MOST WIEDZY Downloaded from mostwiedzy.pl

obviously evident, especially for AHP as microparticles, because $Al_2(HPO_4)_3$ degraded to aluminum pyrophosphate [$Al_4(P_2O_7)_3$] and released water [30,33]. Interestingly, at the temperature of 600 °C, the residual product (mainly containing $Al_4(P_2O_7)_3$ [43]) was slightly higher in the case of AHP NPs than for as received AHP microparticles (in the same order with the value 80% vs. 71%).

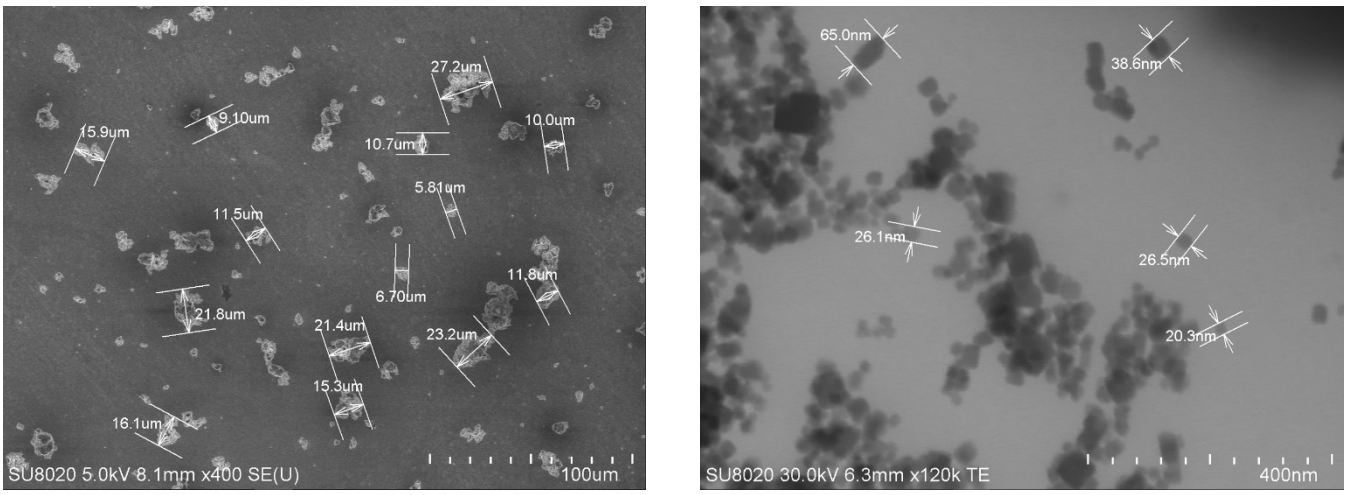

(**a**) (**b**)

Figure 1. (**a**,**b**). Selected images of AHP before and after grinding: (**a**) SEM of as-received microparticles before grinding; (**b**) STEM of nanoparticles obtained by the two successive grindings.

Table 1. TGA results obtained following the characterization of AHP (micro- and nanoparticles) under nitrogen and air.

Sample	Gas	$T_{5\%}$, °C	T_{d1}, °C	T_{d2}, °C	Residual Product at 600 °C, %
AHP (micrometric)	N_2	353	361	451	71
AHP (nanometric)	N_2	332	344	~460	81
AHP (micrometric)	air	ND *	322	442	84
AHP (nanometric)	air	ND *	298	~440	85

* Not determined (ND)/exothermal reaction of PH_3 in air with effects on the accuracy of the measurements.

Scheme 1 suggests the mechanism of thermal degradation of AHP under nitrogen which is generally agreed in the literature [30,43]. Under nitrogen atmospher, in relation to the FR effects of AHP, is noted the formation of phosphine (reaction 1) and of water (reaction 2) as the main components of the gas phase, produced respectively, in the first and second stages of degradation. The degradation pathway described in Scheme 1 does not appear appropriate for AHP nanoparticles since the second decomposition step, corresponding to water loss, does not occur when AHP NANO are analyzed. Reduced particle size, from micro to nanoscale, has a significant impact on AHP's thermal behavior. To explain the difference in mass residue between both particles, a detailed study of the thermal behavior of AHP NPs is required. Additionally, this will explain why AHP NPs appear to gain mass during the second decomposition step.

Apparently, based on the TGA investigations, the AHP NPs are more sensitive to the thermal degradation, under both nitrogen and air atmospheres (TGA data are summarized in Table 1).

MOST WIEDZY Downloaded from mostwiedzy.pl

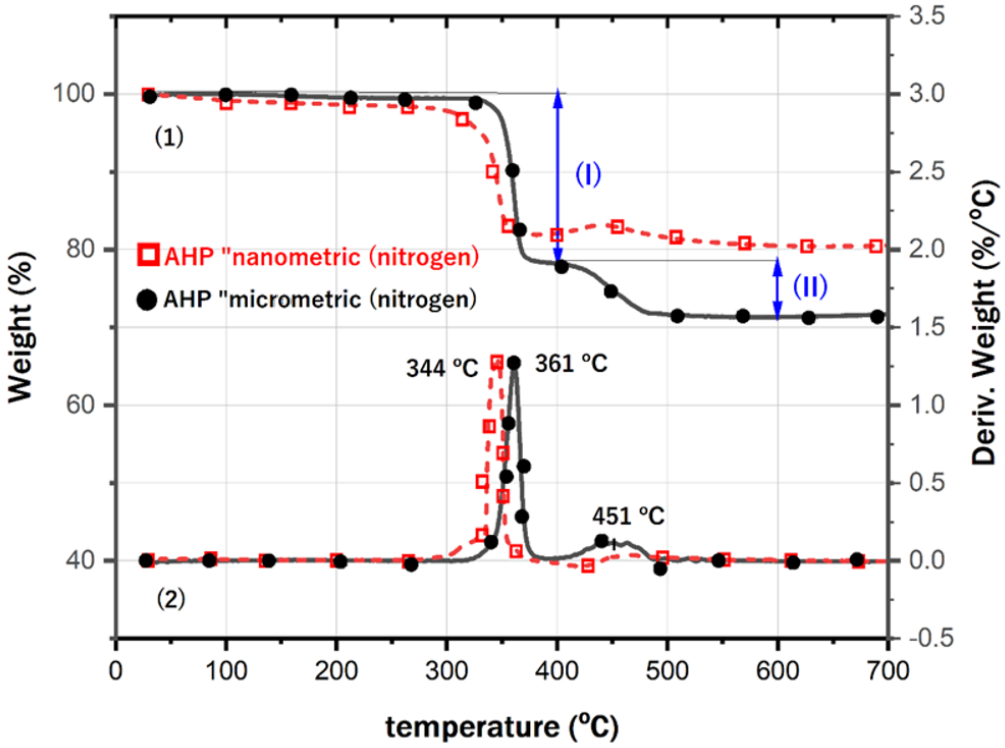

Figure 2. Comparative (1) TG and (2) DTG traces of AHP micro- and nanoparticles conditioned in N_2 atmosphere (heating rate: 20 °C/min).

Under N_2

$$2Al(H_2PO_2)_3 \longrightarrow Al_2(HPO_4)_3 + PH_3 \quad (1)$$

$$2Al_2(HPO_4)_3 \longrightarrow Al_4(P_2O_7)_3 + 3H_2O \quad (2)$$

Scheme 1. Proposed mechanism of thermal decomposition of AHP under nitrogen.

On the other hand, as Figure 3a,b suggests, AHP presented a different thermal degradation pathway under air compared with the one under nitrogen. Due to their higher surface area, NPs are assumed to improve heat transfer comparatively to microparticles, which is in agreement with the slightly lower degradation temperature observed for AHP NPs. Noteworthy the highest rate of degradation under air was seen at about 300 °C and 320 °C, respectively, which can be ascribed to the formation/liberation of PH_3 and its transfer to the gas phase. However, from the shape of TG curves (Figure 3a) a peculiar unexpected behavior was seen, with impact also on the DTG traces (curves not shown here). Based on our best knowledge, it appears that this thermal behavior of AHP under air/oxygen was less discussed in the previous papers or dissimilar results were reported [30,37]. To obtain more insight, Figure 3b shows the evolution of the weight and measured temperature of the samples (NB: by the thermocouple of the apparatus), as function of the time of heating, at constant heating rate of 20 °C/min. Accordingly, it is revealed that the quick formation/weight loss of PH_3 (NB: during a very short time), which is the product formed in the first stage of degradation (Scheme 2, reaction 1), has some collateral consequences on the accuracy of TG measurements due to the high reactivity of phosphine with the oxygen from air. However, it is well known that the reaction of phosphine with the oxygen (in air) is highly exothermic (mixtures of phosphine and oxygen could even explode spontaneously [44]); therefore, high deviations from the programmed temperature were seen, i.e., dramatical increases in the measured temperature to above 400 °C and 456 °C, for NPs and

MOST WIEDZY Downloaded from mostwiedzy.pl

microparticles, respectively. On the other hand, a higher amount of char (i.e., 84%–85%) was determined as residual product following the thermal degradation of AHP under air.

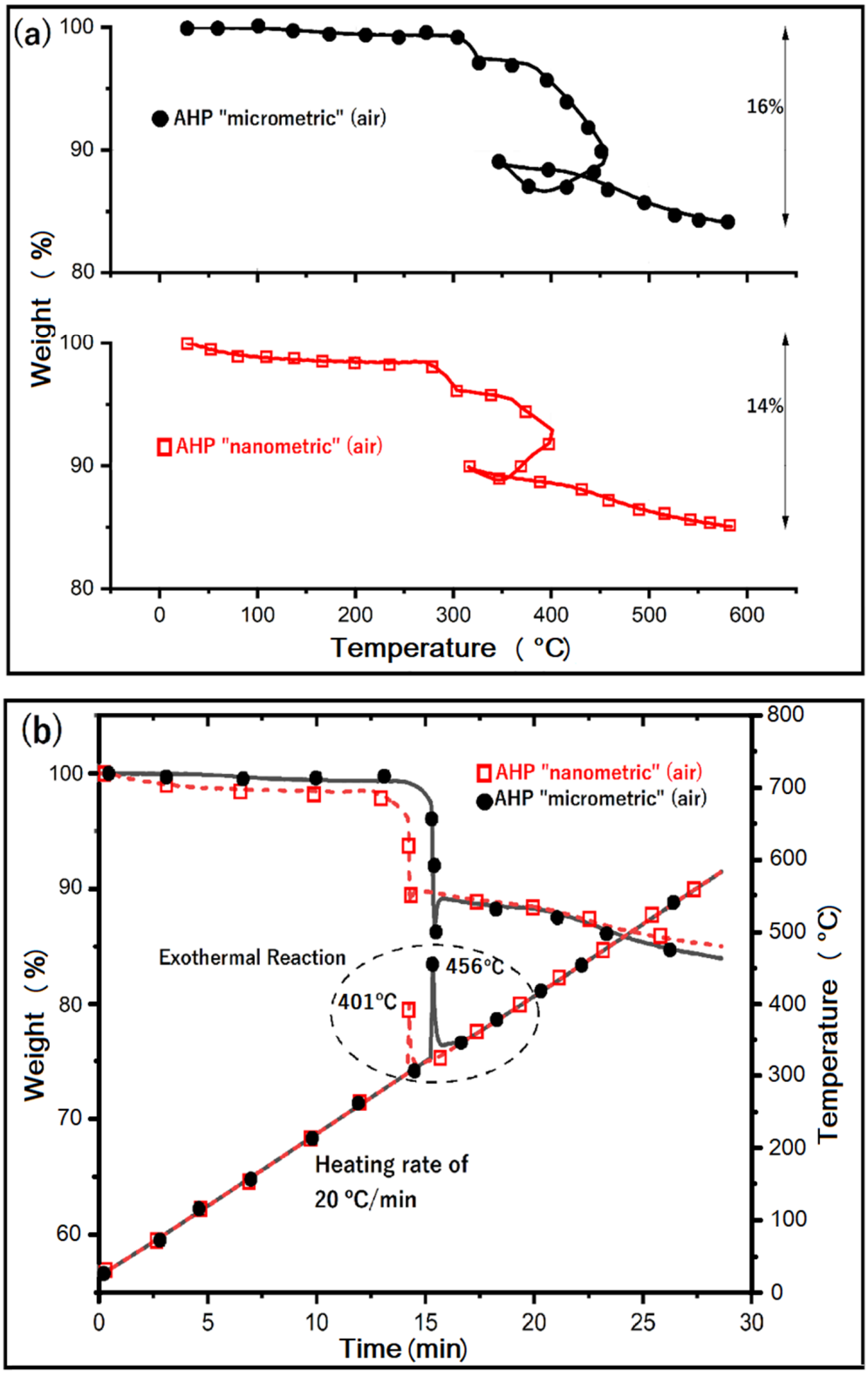

Figure 3. (**a**,**b**). Comparative TGA of AHP microparticles and NPs under air: (**a**) evolution of the weight function of temperature; (**b**) evolution of the weight and measured temperature during the time of heating (heating rate: 20 °C/min).

MOST WIEDZY Downloaded from mostwiedzy.pl

Under air

$$2Al(H_2PO_2)_3 \longrightarrow Al_2(HPO_4)_3 + 3PH_3 \quad (1)$$

$$Al(H_2PO_2)_3 + 3O_2 \longrightarrow Al(PO_3)_3 + 3H_2O \quad (1')$$

$$2Al_2(HPO_4)_3 \longrightarrow Al_4(P_2O_7)_3 + 3H_2O \quad (2)$$

$$PH_3 + 2O_2 \longrightarrow H_3PO_4 \quad (3)$$

$$nH_3PO_4 \longrightarrow \text{polyphosphoric acid} + \text{water} \quad (4)$$

Scheme 2. Proposed mechanism and main reactions of thermal decomposition of AHP under air.

Scheme 2 suggests a mechanism for the thermal degradation of AHP under air (oxidative) condition. First, it is important to mention that there are some differences between the mechanisms proposed in the literature, mostly arising from the specificity of techniques/conditions of analysis, but also because of the multiple chemical transformations, which can be attributed to aluminum/phosphorus-based products. Generally, it is agreed that the decomposition of AHP follows almost similar pathways/thermal changes such as under nitrogen (reactions 1 and 2), with the formation of phosphine and water as volatiles, respectively. On the other hand, according to some authors (e.g., Zhao et al. [43]), AHP reacts first with the oxygen (reaction 1′) leading to formation of aluminum metaphosphate ($Al(PO_3)_3$) and water. However, the formation (reaction 1) and oxidation of phosphine to phosphoric acid, and its ulterior transformation into polyphosphoric acid (reactions 3 and 4, respectively), are mentioned in the majority of reports [30]. Formation of aluminum phosphate ($AlPO_4$) and the release of other volatile products (not mentioned in Scheme 2), including hypophosphorous acid (H_3PO_2) and red phosphorus (P_4), was also reported [31]. Still, it is considered that the mass increase of the residue under air may result from the oxidation of AHP [43].

Linked to the FR action of AHP in air, it is highly agreed that the water vapor molecules formed during thermal degradation of AHP dilute the oxygen and combustible gases, while phosphine (PH_3) is converted to phosphorous acids through oxidation, which provides support for stable/intumescent structures with the different polymers, in the condensed phase [32]. Moreover, following the synergies with the aluminum salts formed in the process of degradation/transformation of AHP, these structures could lead to compact/cross-linked char layers [33,34,36], which are significantly inhibiting mass and heat transfer, with effects in retarding the burning process. On the other hand, phosphine and its derivatives are radical scavengers that trap the radicals needed for combustion. Phosphine produces phosphorus-based radicals ($PO_2\cdot$, $PO\cdot$, etc.) in the flame zone that trap H· and HO· radicals from the gas phase, therefore leading to fewer flammable products for combustion [45]. Ultimately, in the case of FR polymeric composites containing AHP, it is assumed that the gas phase activity and formation of stable charring structures could act together for the enhancement of FR properties [32,39].

3.2. Characterization of Epoxy/AHP Nanocomposites

The thermal stability of epoxy/AHP nanocomposites was investigated under anaerobic condition in order to study the materials pyrolysis which is the main degradation pathway after ignition in the condensed phase. Figure 4 shows the comparative TG curves of neat epoxy resin and epoxy/AHP nanocomposites under nitrogen atmosphere, besides the corresponding data from the thermal analysis are listed in Table 2. Neat epoxy thermal degradation occurred in two stages; (i) the first stage (150–275 °C) showing around 5%

MOST WIEDZY Downloaded from mostwiedzy.pl

mass loss attributed to the loss of water via dehydration and eventual traces of solvent, followed by (ii) statistical rupture of the epoxy resin structure to form a char of about 11.8%. The first degradation step is mainly observed in the case of uncurred epoxy resin and corresponding to the condensation of curing agent during which some dehydration and elimination of low molecular weight molecules occurs [46].

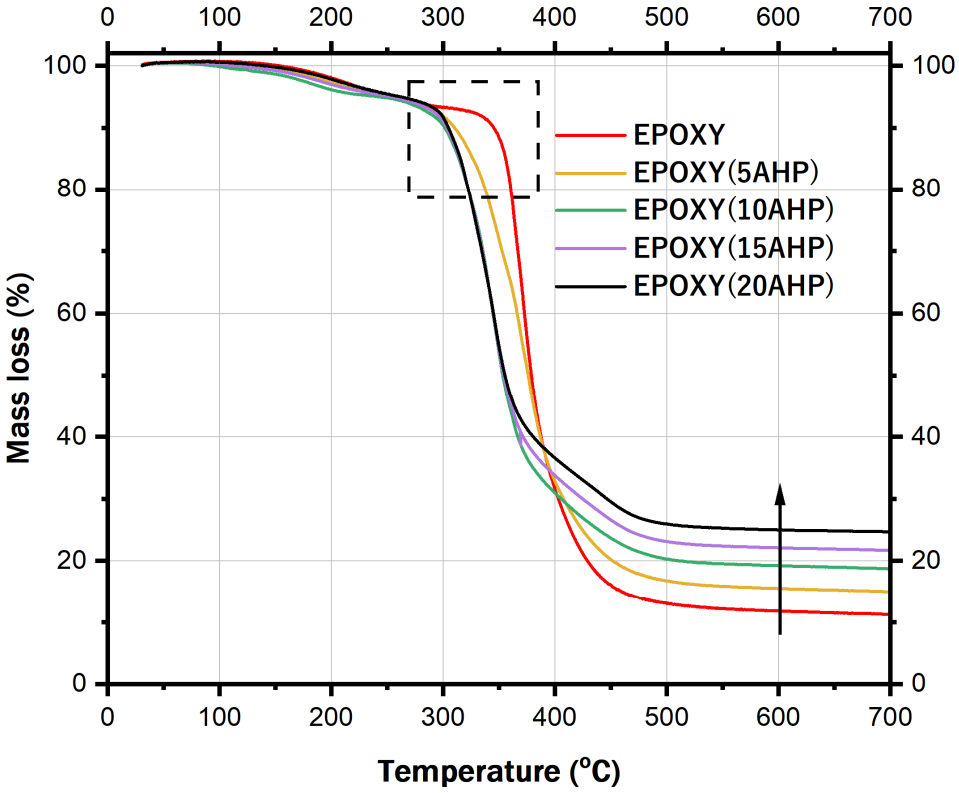

Figure 4. Comparative TG traces of epoxy/AHP nanocomposites and blank epoxy resin under nitrogen (heating rate: 10 °C/min).

Table 2. TGA data obtained following the characterization of epoxy/AHP nanocomposites under nitrogen.

Sample	$T_{10\%}$, °C	$T_{50\%}$, °C	T_d, °C	Residual Product at 600 °C, %
Neat epoxy	350	384	378	11.8
Epoxy (5AHP)	310	376	377	15.5
Epoxy (10AHP)	301	353	347	19.2
Epoxy (15AHP)	305	354	346	22.1
Epoxy (20AHP)	305	355	349	25.0

All curves showed only one weight loss stage, and the predominant degradation process was mainly evidenced between 300 °C and 400 °C, following the degradation of AHP and of epoxy matrix, observed at much higher temperature. However, especially by considering the values of temperature at weight loss of 10% and 50% ($T_{10\%}$ and $T_{50\%}$, respectively), it turned out that AHP made no contribution to the improvement in thermal properties of epoxy resin. $T_{10\%}$ of epoxy (350 °C) appeared to be significantly higher than that of nanocomposites (300–310 °C). This is explained by the specific behavior of AHP at high temperatures (as discussed in the previous section), which is finally connected to its action as FR additive. Similar reduction in thermal stability of nanocomposite induced by the presence of AHP was also observed by Gu et al. [29] for PLA. By contrary, increasing the content of nanofiller in nanocomposites is well correlated with the progressive growing of the residual products, e.g., from about 12% (neat epoxy) to 25% (epoxy/20% AHP

MOST WIEDZY Downloaded from mostwiedzy.pl

nanocomposites). The amount of the final residue, generated during the TGA under nitrogen, increased with increasing AHP NPs content.

The flammability behavior of samples was evaluated using PCFC. Heat release curves as a function of temperature are given in Figure 5; besides, Table 3 summarizes the main parameters obtained from PCFC test including pHRR and its corresponding temperature (T_{pHRR}). Blank epoxy was burnt in one main step and its pHRR was 550 W/g at 386 °C. It is clear that the presence of AHP even at very low content (1 wt.%) affects significantly the flammability pathway of epoxy, as understood from a fall in the value of T_{pHRR} from 386 °C to 354 °C. This important reduction is in good correlation with TGA results (Figure 4) that evidenced degradant effect of AHP NPs on epoxy resin. At 5 wt.% AHP NPs content, similar behavior was observed. However, the pHRR of both nanocomposites (1 and 5 wt.%) remained almost close to that of neat epoxy. Of note, a different behavior was observed for the samples containing 10 and 20 wt.% AHP. These nanocomposites demonstrated a significant decrease in pHRR to 385 and 346 W/g, respectively, showing a better flammability resistance.

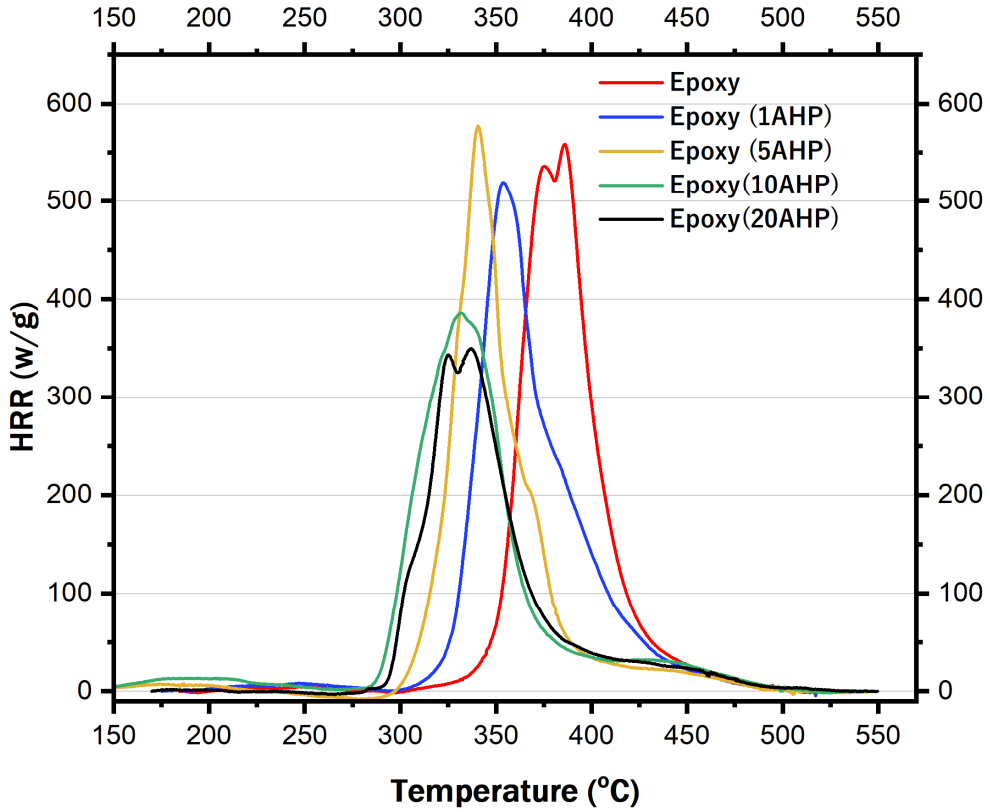

Figure 5. Heat release rate (HRR) curves vs. the temperature of neat epoxy and epoxy/AHP nanocomposites obtained by PCFC analysis.

Table 3. The values of peak of heat release rate (pHRR) and temperature at the peak of the heat release rate (T_{pHRR}) obtained by PCFC analysis.

Sample	pHRR, W/g	T_{pHRR}, °C
Neat epoxy	550	386
Epoxy (1AHP)	520	354
Epoxy (5AHP)	573	340
Epoxy (10AHP)	385	333
Epoxy (20AHP)	346	338

MOST WIEDZY Downloaded from mostwiedzy.pl

3.3. FR Properties of PLA Sheets Coated with Epoxy/AHP Nanocomposites

Figure 6 shows images of PLA plates, covered by epoxy nanocomposite coatings of 100 µm thickness, containing 5, 10, 15 and 20 wt.% AHP NPs. From these images, one can observe that the epoxy coating remained transparent despite the addition of AHP NPs, at a relatively high incorporation content of 20 wt.%. Several cracks can also be observed in the layer of epoxy coating containing 20% AHP. However, the surface aspect of coatings obtained with epoxy/AHP nanocomposites can be considered as a promising achievement, since the incorporation of FR additives into polymers generally negatively affects the mechanical properties and transparency.

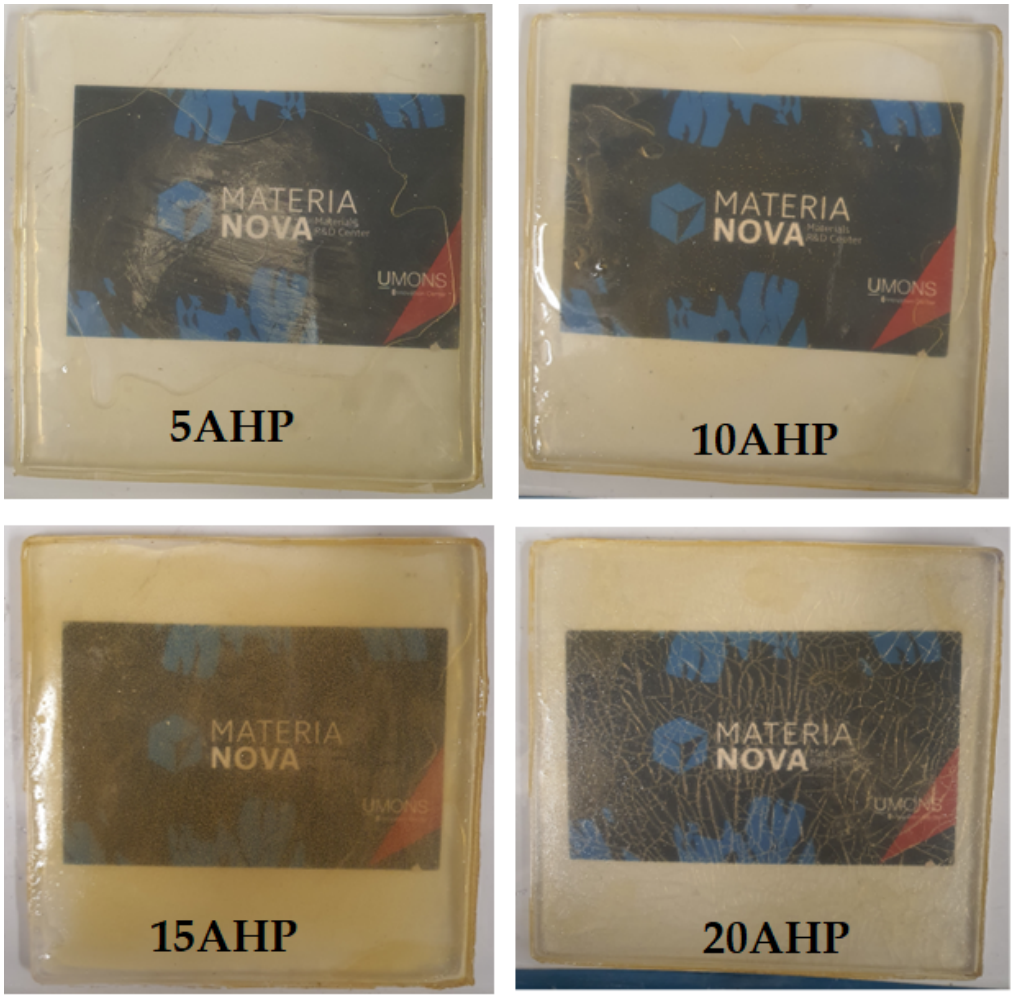

Figure 6. PLA plates surface coated with epoxy/AHP nanocomposite films containing 5, 10, 15 and 20 wt.% AHP nanoparticles.

As shown in Figure 7, these coatings are transparent due to the high quality of dispersion/distribution of the small AHP NPs into epoxy resin. Additionally, it confirms the efficacy of the mixing process used (see Section 2.4). Since the loading of AHP was high, i.e., 20 wt.%, we can also observe the presence of few micrometric aggregates of very small size (<1 µm), which testify to the high degree of interaction between the NPs (NB: here used without any surface treatment). Overall, most NPs were well dispersed in the epoxy matrix.

MOST WIEDZY Downloaded from mostwiedzy.pl

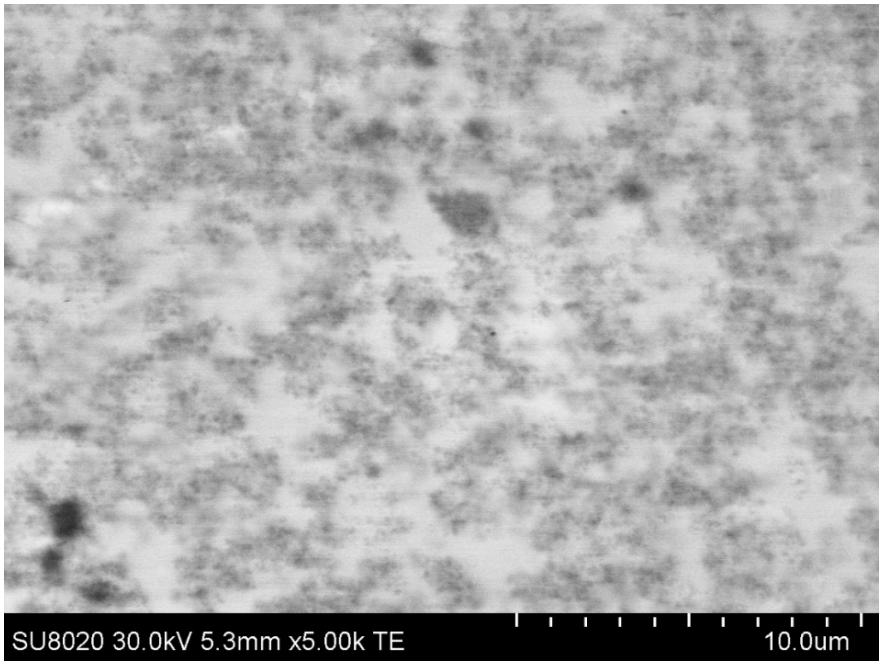

Figure 7. STEM image of epoxy nanocomposite coating containing 20 wt.% AHP NPs.

3.3.1. Mass Loss Cone Calorimeter Tests

The fire behavior of the different PLA coated plates was evaluated using MLC, which is considered as the most widely used device to assess the fire behavior of materials at bench scale. Samples were submitted to a heat flux of 35 kW/m^2, corresponding to common heat flux in a mild fire scenario. We took into consideration both the pHRR and the TTI, which are considered as two of the most important parameters in this fire test. In fact, fast ignition and rapid-fire propagation can both result from a high pHRR and low TTI. Curves of the MLC test are presented Figure 8 and results are summarized in Table 4.

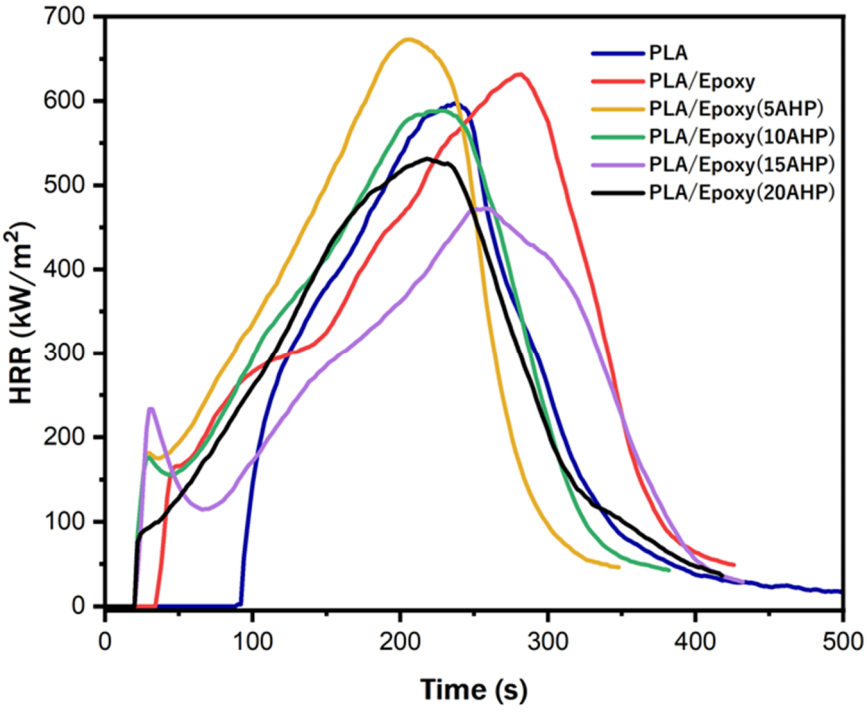

Figure 8. Heat release rate (HRR) obtained in MLC test of PLA (sheets) coated with epoxy–AHP nanocomposites compared to PLA/blank epoxy resin and pristine PLA.

MOST WIEDZY Downloaded from mostwiedzy.pl

Table 4. MLC data (35 kW/m^2).

Sample	TTI, (s)	pHRR (kW/m^2)	pHRR Variation (%)	THR (kW/m^2)
PLA	92	584	-	100
PLA/Epoxy	34	612	+4.8	132
PLA/Epoxy(5AHP)	20	640	+9.6	114
PLA/Epoxy(10AHP)	19	546	−6.5	113
PLA/Epoxy(15AHP)	20	435	−25.5	107
PLA/Epoxy(20AHP)	21	490	−16.0	107

For a correct estimation of the FR effect of epoxy coatings containing AHP NPs, two PLA-based reference sheets were used for comparison, i.e., (i) uncoated PLA sheets and (ii) PLA sheets coated with blank epoxy resin.

Pristine PLA exhibited a strong combustion, starting after 92 s, consuming all the material with a pHRR of 584 kW/m^2. The epoxy coating had a negative effect on PLA combustion, since TTI decreased from 92 s to 34 s, while pHRR increased by 4.8%, from 584 to 612 kW/m^2. Epoxy resins, such as diglycidyl ether of bisphenol A (DGEBA) used in our study, are highly flammable (we chose it to assess the effect of the AHP on the coating) [47,48] and their use solely could not provide any FR protection to PLA plates. Nevertheless, epoxy-coated PLA exhibited a slightly different HRR curve shape than uncoated PLA. It seems that a residue was formed on the surface of the material during combustion, since the TTI was slightly reduced (around 45 s) at the beginning of combustion.

The degraded epoxy coating formed an ephemeral barrier at the beginning of the combustion. This barrier degraded rapidly and HRR continued to grow and reach higher pHRR than that obtained with neat PLA sample.

The incorporation of AHP NPs, whatever their incorporation content, induced a further reduction in the TTI such that it decreased to 20 s. This is in good agreement with the results obtained in both TGA and PCFC analyses, which demonstrated that the addition of even small amount of AHP NPs triggers significant reduction in the epoxy thermal stability.

AHP nanoparticles incorporated into epoxy coatings considerably affected the fire behavior of coated PLA sheets in MLC tests (Figure 8). At a low incorporation level (5 wt.%), the efficiency of the protective barrier formed by the epoxy remained very low and did not allow any reduction of the HRR release level, whose maximum exceeded the value recorded for the neat PLA. Even at 10 wt.%, the HRR remains out of control. The presence of AHP NPs did not allow any FR effect, except a more marked decrease in the HRR at the beginning of the combustion. At 5 and 10 wt.%, the AHP content was not high enough to ensure a fully developed char layer at the surface at an early stage of the combustion. In contrast, at 15 wt.%, AHP NPs produced a more pronounced FR effect and better HRR control. A major reduction in the HRR was observed after the ignition, due to the formation of a char layer that prevents the HRR growth until the layer cracks. The reduction of the TTI observed is due to the reaction between phosphoric acid, generated during AHP thermal decomposition, and epoxy resin. As it has been shown by both TGA (Figure 4) and PCFC (Figure 5) analysis, the presence of AHP NPs induces premature thermal degradation of epoxy resin. This reaction leads to the generation of volatile compounds, including phosphine, but also leads to the formation of a char layer responsible for the first HRR peaks occurring just after the ignition.

A second HRR growth was thus observed after 80 s until reaching the lowest pHRR obtained in our study (435 kW/m^2, −25.5%). A higher incorporation AHP amount (20 wt.%) led to a disappearance of the first peak of heat release rate and to a slightly higher pHRR level than that obtained with 15 wt.% AHP NPs. It appears that the poor quality of this coating contributed to this result, as evidenced in Figure 6 by the numerous cracks present on the surface of sample.

MOST WIEDZY Downloaded from mostwiedzy.pl

The total heat release (THR) was not significantly reduced in the presence of AHP. First, it is critical to note that the deposition of the virgin epoxy layer significantly increased the THR from 100 for PLA alone to 130 MJ/m^2. Adding 15 and 20% AHP NPs gradually reduced this value to about 107. The THR values of the latter two compositions remained at the same level as that of pristine PLA. However, we can also notice that pHRR decreased and heat is released over a longer time range. It should also be noted that the use of an epoxy layer, which is itself combustible, on PLA plates led to an increase in the amount of combustible material tested. This can greatly affect the THR.

These results showed that the achievement of an appropriate fire protection effect by epoxy coating is essentially conditioned by two elements, (1) adequate amount of AHP NPs that enables a system to intensify charring and (2) a homogeneous coating without cracks. The images of the specimens at the end of the combustion test (Figure 9) indicated that the sample containing 15 wt.% AHP NPS on the top coating layer of epoxy is the one solely meets both above-mentioned quality criteria (sufficient amount of AHP and the absence of cracks). This is reflected in the amount of the charred residue at the end of the experiment.

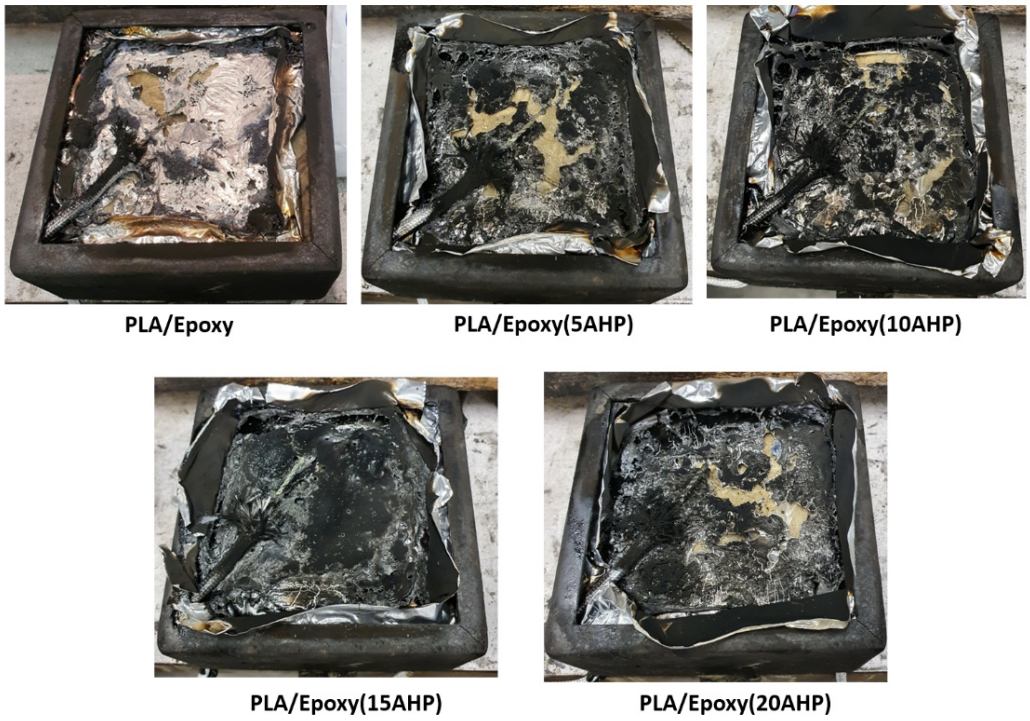

Figure 9. Pictures taken from samples to illustrate the aspect of residual products after MLC testing.

3.3.2. Protective and Insulating Effect of Epoxy-AHP Coatings

The protective and insulating effect of the residue formed with 15 wt.% AHP NPs is also revealed by monitoring the temperature evolution of the unexposed face of the plates during the cone calorimeter test. Figure 10 shows the evolution of the temperature as a function of time on the unexposed uncoated PLA side. The PLA/Epoxy (15AHP) composition was the only one that provides a more effective insulating effect. Indeed, the temperature of the unexposed side of PLA/Epoxy (15AHP) plates reached a maximum of 430 °C after 400 s of exposure, while this temperature exceeded 500 °C from 300 s in the case of the other compositions. This result additionally confirmed that the epoxy coating at 15 wt.% AHP NPs was more efficient thanks to the absence of cracks and also due to a better charring protection during the combustion.

MOST WIEDZY Downloaded from mostwiedzy.pl

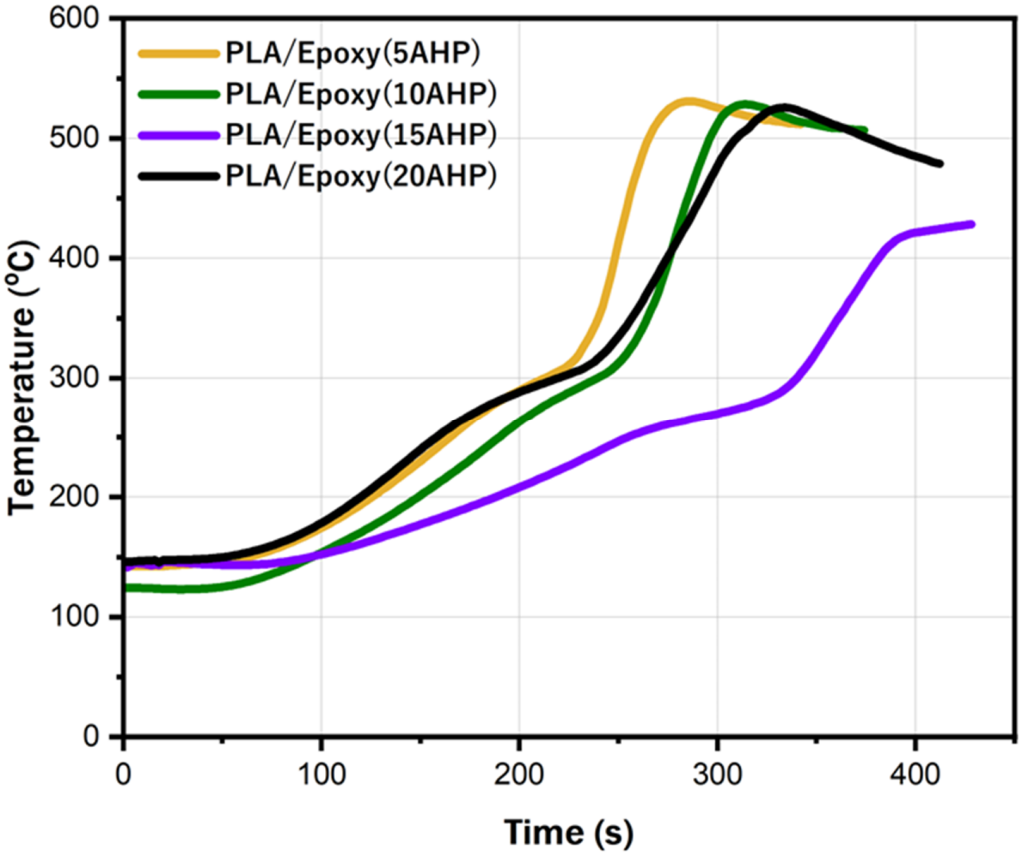

Figure 10. The evolution of the temperature at the non-exposed sides of the plates during cone calorimeter test (35 kW/m^2).

Based on the above analysis, Figure 11 summarizes the protective flame-retardant effect of epoxy coating containing the AHP NPs, at the surface of PLA sheets.

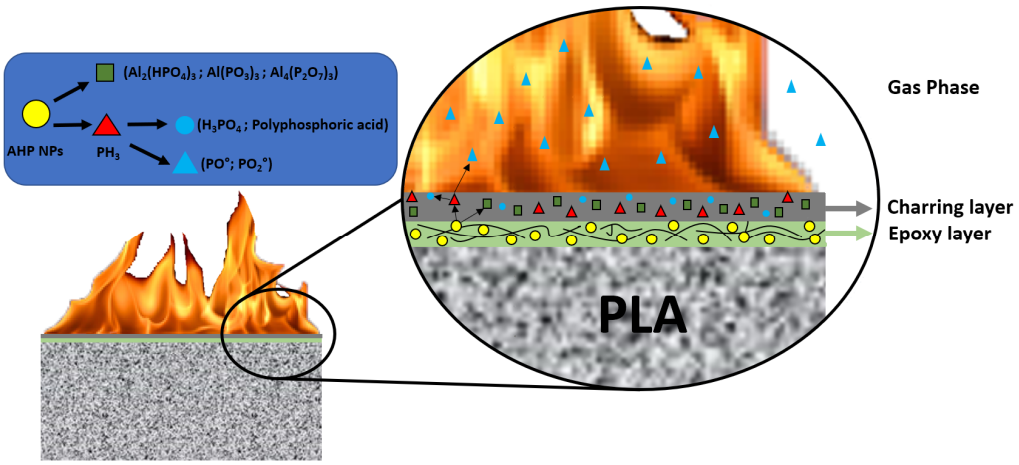

Figure 11. Schematic illustration for the flame-retardant mechanism of PLA/Epoxy-AHP NPs composites.

4. Conclusions

The present study provided an appropriate solution to current requests regarding the development of transparent non-halogenated FR coatings with a dual role, decorative (transparent) and protective (fire-retardant). AHP NPs were successfully dispersed and distributed within epoxy to prepare transparent nanocomposite coatings containing 5, 10, 15, and 20 wt.% AHP, as was evidenced by SEM and STEM images. The thermal

MOST WIEDZY Downloaded from mostwiedzy.pl

stability and FR effect of these coatings were evaluated under different gas atmospheres, and possible mechanisms of thermal degradation and flame retardancy were discussed. With the increase of AHP NPs content from 5 to 20 wt.%, the thermal stability of the coatings decreased as the result of the chemical reaction between the products formed through AHP NPs degradation (phosphoric acid, water molecules) and epoxy. This interaction, as well as the low thermal stability of AHP NPS, proved responsible for the reduction in the TTI of the coated PLA plates during cone calorimeter test. However, under specific conditions (15 wt.% AHP NPs and the absence of cracks), the epoxy coating was able to ensure a significant reduction in the pHRR and appropriate insulating thermal properties of coated PLA plates.

Author Contributions: Conceptualization, F.L. and H.V.; methodology, M.J., O.M. and M.M.; validation, L.B. and P.D.; formal analysis, L.B.; investigation, F.L. and H.V.; data curation, F.L. and M.M.; writing—original draft preparation, F.L., M.M., P.D. and M.J.; writing—review and editing, H.V. and M.R.S.; visualization, H.V. and M.R.S.; supervision, F.L. All authors have read and agreed to the published version of the manuscript.

Funding: This research received no external funding.

Institutional Review Board Statement: Not applicable.

Informed Consent Statement: Not applicable.

Data Availability Statement: Data available based on request.

Conflicts of Interest: The authors declare no conflict of interest.

References

1. Wang, K.; Liu, H.; Wang, C.; Huang, W.; Tian, Q.; Fu, Q.; Yan, W. Flame-Retardant Performance of Epoxy Resin Composites with SiO2 Nanoparticles and Phenethyl-Bridged DOPO Derivative. *ACS Omega* **2021**, *6*, 666–674. [CrossRef] [PubMed]
2. Ahmadi, Z. Nanostructured Epoxy Adhesives: A Review. *Prog. Org. Coat.* **2019**, *135*, 449–453. [CrossRef]
3. Jouyandeh, M.; Jazani, O.M.; Navarchian, A.H.; Shabanian, M.; Vahabi, H.; Saeb, M.R. Bushy-Surface Hybrid Nanoparticles for Developing Epoxy Superadhesives. *Appl. Surf. Sci.* **2019**, *479*, 1148–1160. [CrossRef]
4. Shen, D.; Xu, Y.-J.; Long, J.-W.; Shi, X.-H.; Chen, L.; Wang, Y.-Z. Epoxy Resin Flame-Retarded via a Novel Melamine-Organophosphinic Acid Salt: Thermal Stability, Flame Retardance and Pyrolysis Behavior. *J. Anal. Appl. Pyrolysis* **2017**, *128*, 54–63. [CrossRef]
5. Wang, P.; Xia, L.; Jian, R.; Ai, Y.; Zheng, X.; Chen, G.; Wang, J. Flame-Retarding Epoxy Resin with an Efficient P/N/S-Containing Flame Retardant: Preparation, Thermal Stability, and Flame Retardance. *Polym. Degrad. Stab.* **2018**, *149*, 69–77. [CrossRef]
6. Vahabi, H.; Jouyandeh, M.; Cochez, M.; Khalili, R.; Vagner, C.; Ferriol, M.; Movahedifar, E.; Ramezanzadeh, B.; Rostami, M.; Ranjbar, Z.; et al. Short-Lasting Fire in Partially and Completely Cured Epoxy Coatings Containing Expandable Graphite and Halloysite Nanotube Additives. *Prog. Org. Coat.* **2018**, *123*, 160–167. [CrossRef]
7. Bifulco, A.; Varganici, C.; Rosu, L.; Mustata, F.; Rosu, D.; Gaan, S. Recent Advances in Flame Retardant Epoxy Systems Containing Non-Reactive DOPO Based Phosphorus Additives. *Polym. Degrad. Stab.* **2022**, *200*, 109962. [CrossRef]
8. Ratna, D. *Epoxy Composites: Impact Resistance and Flame Retardancy*; Rapra review reports; Rapra Technology Ltd.: Billingham, UK, 2005, ISBN 978-1-62870-908-7.
9. Yan, W.; Xie, P.; Yang, Z.; Luo, G.; Huang, W.; Tian, Q.; Tu, C.; Zhang, C.; Yang, C.; Wang, K. Flame-Retardant Behaviors of Aluminum Phosphates Coated Sepiolite in Epoxy Resin. *J. Fire Sci.* **2021**, *39*, 3–18. [CrossRef]
10. Xu, B.; Liu, Y.; Wei, S.; Zhao, S.; Qian, L.; Chen, Y.; Shan, H.; Zhang, Q. A Phosphorous-Based Bi-Functional Flame Retardant Based on Phosphaphenanthrene and Aluminum Hypophosphite for an Epoxy Thermoset. *Int. J. Mol. Sci.* **2022**, *23*, 11256. [CrossRef]
11. Huo, S.; Song, P.; Yu, B.; Ran, S.; Chevali, V.S.; Liu, L.; Fang, Z.; Wang, H. Phosphorus-Containing Flame Retardant Epoxy Thermosets: Recent Advances and Future Perspectives. *Prog. Polym. Sci.* **2021**, *114*, 101366. [CrossRef]
12. Movahedifar, E.; Vahabi, H.; Saeb, M.R.; Thomas, S. Flame Retardant Epoxy Composites on the Road of Innovation: An Analysis with Flame Retardancy Index for Future Development. *Molecules* **2019**, *24*, 3964. [CrossRef] [PubMed]
13. Abdi, A.A.; Jouyandeh, M.; Vahabi, H.; Shabanian, M.; Lafon-Pham, D.; Gabrion, X.; Laheurte, P.; Nahavandi, A.M.; Saeb, M.R. Correlating the Photophysical Properties with the Cure Index of Epoxy Nanocomposite Coatings. *J. Inorg. Organomet. Polym. Mater.* **2021**, *31*, 923–933. [CrossRef]
14. Sari, M.G.; Saeb, M.R.; Shabanian, M.; Khaleghi, M.; Vahabi, H.; Vagner, C.; Zarrintaj, P.; Khalili, R.; Paran, S.M.R.; Ramezanzadeh, B.; et al. Epoxy/Starch-Modified Nano-Zinc Oxide Transparent Nanocomposite Coatings: A Showcase of Superior Curing Behavior. *Prog. Org. Coat.* **2018**, *115*, 143–150. [CrossRef]

MOST WIEDZY Downloaded from mostwiedzy.pl

15. Rastin, H.; Saeb, M.R.; Nonahal, M.; Shabanian, M.; Vahabi, H.; Formela, K.; Gabrion, X.; Seidi, F.; Zarrintaj, P.; Sari, M.G.; et al. Transparent Nanocomposite Coatings Based on Epoxy and Layered Double Hydroxide: Nonisothermal Cure Kinetics and Viscoelastic Behavior Assessments. *Prog. Org. Coat.* **2017**, *113*, 126–135. [CrossRef]
16. Teles, F.; Martins, G.; Antunes, F. Fire Retardancy in Nanocomposites by Using Nanomaterial Additives. *J. Anal. Appl. Pyrolysis* **2022**, *163*, 105466. [CrossRef]
17. Laoutid, F.; Bonnaud, L.; Alexandre, M.; Lopez-Cuesta, J.-M.; Dubois, P. New Prospects in Flame Retardant Polymer Materials: From Fundamentals to Nanocomposites. *Mater. Sci. Eng. R Rep.* **2009**, *63*, 100–125. [CrossRef]
18. Murariu, M.; Laoutid, F.; Dubois, P.; Fontaine, G.; Bourbigot, S.; Devaux, E.; Campagne, C.; Ferreira, M.; Solarski, S. Chapter 21—Pathways to Biodegradable Flame Retardant Polymer (Nano)Composites. In *Polymer Green Flame Retardants*; Papaspyrides, C.D., Kiliaris, P., Eds.; Elsevier: Amsterdam, The Netherlands, 2014; pp. 709–773, ISBN 978-0-444-53808-6.
19. Murariu, M.; Dechief, A.L.; Bonnaud, L.; Paint, Y.; Gallos, A.; Fontaine, G.; Bourbigot, S.; Dubois, P. The Production and Properties of Polylactide Composites Filled with Expanded Graphite. *Polym. Degrad. Stab.* **2010**, *95*, 889–900. [CrossRef]
20. Horrocks, R.; Sitpalan, A.; Zhou, C.; Kandola, B.K. Flame Retardant Polyamide Fibres: The Challenge of Minimising Flame Retardant Additive Contents with Added Nanoclays. *Polymers* **2016**, *8*, 288. [CrossRef]
21. Feyz, E.; Jahani, Y.; Esfandeh, M. Effect of a Nanoclay/Triphenyl Phosphate Hybrid System on the Fire Retardancy of Polycarbonate/Acrylonitrile–Butadiene–Styrene Blend. *J. Appl. Polym. Sci.* **2011**, *120*, 3435–3442. [CrossRef]
22. Pack, S.; Si, M.; Koo, J.; Sokolov, J.C.; Koga, T.; Kashiwagi, T.; Rafailovich, M.H. Mode-of-Action of Self-Extinguishing Polymer Blends Containing Organoclays. *Polym. Degrad. Stab.* **2009**, *94*, 306–326. [CrossRef]
23. Wu, H.; Ortiz, R.; Correa, R.D.A.; Krifa, M.; Koo, J.H. Self-Extinguishing and Non-Drip Flame Retardant Polyamide 6 Nanocomposite: Mechanical, Thermal, and Combustion Behavior. *Flame Retard. Therm. Stab. Mater.* **2018**, *1*, 1–13. [CrossRef]
24. Swoboda, B.; Leroy, E.; Laoutid, F.; Lopez-Cuesta, J.-M. Flame-Retardant PET-PC Blends Compatibilized by Organomodified Montmorillonites. In *Fire and Polymers V*; ACS Symposium Series; American Chemical Society: Washington DC, USA, 2009; Volume 1013, pp. 83–101. ISBN 978-0-8412-6988-0.
25. Kalali, E.N.; Wang, X.; Wang, D.-Y. Multifunctional Intercalation in Layered Double Hydroxide: Toward Multifunctional Nanohybrids for Epoxy Resin. *J. Mater. Chem. A* **2016**, *4*, 2147–2157. [CrossRef]
26. Levchik, S. Phosphorus-Based Flame Retardants. In *Non-Halogenated Flame Retardant Handbook*; John Wiley & Sons: Hoboken, NJ, USA, 2021; pp. 23–99. ISBN 978-1-119-75224-0.
27. Yang, W.; Song, L.; Hu, Y.; Lu, H.; Yuen, R.K.K. Enhancement of Fire Retardancy Performance of Glass-Fibre Reinforced Poly(Ethylene Terephthalate) Composites with the Incorporation of Aluminum Hypophosphite and Melamine Cyanurate. *Compos. Part B Eng.* **2011**, *42*, 1057–1065. [CrossRef]
28. Li, Q.; Li, B.; Zhang, S.; Lin, M. Investigation on Effects of Aluminum and Magnesium Hypophosphites on Flame Retardancy and Thermal Degradation of Polyamide 6. *J. Appl. Polym. Sci.* **2012**, *125*, 1782–1789. [CrossRef]
29. Gu, L.; Qiu, J.; Qiu, C.; Yao, Y.; Sakai, E.; Yang, L. Mechanical Properties and Degrading Behaviors of Aluminum Hypophosphite-Poly(Lactic Acid) (PLA) Nanocomposites. *Polym.-Plast. Technol. Mater.* **2019**, *58*, 126–138. [CrossRef]
30. Tang, G.; Wang, X.; Xing, W.; Zhang, P.; Wang, B.; Hong, N.; Yang, W.; Hu, Y.; Song, L. Thermal Degradation and Flame Retardance of Biobased Polylactide Composites Based on Aluminum Hypophosphite. *Ind. Eng. Chem. Res.* **2012**, *51*, 12009–12016. [CrossRef]
31. Yan, Y.-W.; Huang, J.-Q.; Guan, Y.-H.; Shang, K.; Jian, R.-K.; Wang, Y.-Z. Flame Retardance and Thermal Degradation Mechanism of Polystyrene Modified with Aluminum Hypophosphite. *Polym. Degrad. Stab.* **2014**, *99*, 35–42. [CrossRef]
32. Wu, S.; Deng, D.; Zhou, L.; Zhang, P.; Tang, G. Flame Retardancy and Thermal Degradation of Rigid Polyurethane Foams Composites Based on Aluminum Hypophosphite. *Mater. Res. Express* **2019**, *6*, 105365. [CrossRef]
33. Savas, L.A.; Hacioglu, F.; Hancer, M.; Dogan, M. Flame Retardant Effect of Aluminum Hypophosphite in Heteroatom-Containing Polymers. *Polym. Bull.* **2020**, *77*, 291–306. [CrossRef]
34. Tian, S.; He, H.; Wang, D.; Yu, P.; Jia, Y.; Luo, Y. Study of Using Aluminum Hypophosphite as a Flame Retardant for Low-Density Polyethylene. *Fire Mater.* **2017**, *41*, 983–992. [CrossRef]
35. Velencoso, M.M.; Battig, A.; Markwart, J.C.; Schartel, B.; Wurm, F.R. Molecular Firefighting—How Modern Phosphorus Chemistry Can Help Solve the Challenge of Flame Retardancy. *Angew. Chem. Int. Ed.* **2018**, *57*, 10450–10467. [CrossRef] [PubMed]
36. Zhao, B.; Chen, L.; Long, J.-W.; Chen, H.-B.; Wang, Y.-Z. Aluminum Hypophosphite versus Alkyl-Substituted Phosphinate in Polyamide 6: Flame Retardance, Thermal Degradation, and Pyrolysis Behavior. *Ind. Eng. Chem. Res.* **2013**, *52*, 2875–2886. [CrossRef]
37. Ge, H.; Tang, G.; Hu, W.-Z.; Wang, B.-B.; Pan, Y.; Song, L.; Hu, Y. Aluminum Hypophosphite Microencapsulated to Improve Its Safety and Application to Flame Retardant Polyamide 6. *J. Hazard. Mater.* **2015**, *294*, 186–194. [CrossRef]
38. Savas Atabek, L.; Tayfun, U.; Hancer, M.; Dogan, M. The Flame-Retardant Effect of Calcium Hypophosphite in Various Thermoplastic Polymers. *Fire Mater.* **2019**, *43*, 294–302. [CrossRef]
39. Li, Y.; Jiang, J.; Chen, Z.; Chen, Z.; Ni, L. Preparation and Characterization of Microencapsulated Aluminum Hypophosphite and Its Performance on the Thermal, Flame Retardancy, and Mechanical Properties of Epoxy Resin. *Polym. Compos.* **2021**, *42*, 1818–1834. [CrossRef]
40. Tikhani, F.; Moghari, S.; Jouyandeh, M.; Laoutid, F.; Vahabi, H.; Saeb, M.R.; Dubois, P. Curing Kinetics and Thermal Stability of Epoxy Composites Containing Newly Obtained Nano-Scale Aluminum Hypophosphite (AlPO2). *Polymers* **2020**, *12*, 644. [CrossRef]

MOST WIEDZY Downloaded from mostwiedzy.pl

41. Karami, Z.; Jouyandeh, M.; Ali, J.A.; Ganjali, M.R.; Aghazadeh, M.; Maadani, M.; Rallini, M.; Luzi, F.; Torre, L.; Puglia, D.; et al. Development of Mg-Zn-Al-CO3 Ternary LDH and Its Curability in Epoxy/Amine System. *Prog. Org. Coat.* **2019**, *136*, 105264. [CrossRef]
42. Huggett, C. Estimation of Rate of Heat Release by Means of Oxygen Consumption Measurements. *Fire Mater.* **1980**, *4*, 61–65. [CrossRef]
43. Zhao, P.; Guo, C.; Li, L. Flame Retardancy and Thermal Degradation Properties of Polypropylene/Wood Flour Composite Modified with Aluminum Hypophosphite/Melamine Cyanurate. *J. Therm. Anal. Calorim.* **2019**, *135*, 3085–3093. [CrossRef]
44. Norrish, R.G.W.; Oldershaw, G.A. The Oxidation of Phosphine Studied by Flash Photolysis and Kinetic Spectroscopy. *Proc. R. Soc. Lond. Ser. Math. Phys. Sci.* **1961**, *262*, 10–18.
45. Qu, H.; Liu, X.; Xu, J.; Ma, H.; Jiao, Y.; Xie, J. Investigation on Thermal Degradation of Poly(1,4-Butylene Terephthalate) Filled with Aluminum Hypophosphite and Trimer by Thermogravimetric Analysis–Fourier Transform Infrared Spectroscopy and Thermogravimetric Analysis–Mass Spectrometry. *Ind. Eng. Chem. Res.* **2014**, *53*, 8476–8483. [CrossRef]
46. Kandola, B.K.; Biswas, B.; Price, D.; Horrocks, A.R. Studies on the Effect of Different Levels of Toughener and Flame Retardants on Thermal Stability of Epoxy Resin. *Polym. Degrad. Stab.* **2010**, *95*, 144–152. [CrossRef]
47. Qian, L.; Ye, L.; Qiu, Y.; Qu, S. Thermal Degradation Behavior of the Compound Containing Phosphaphenanthrene and Phosphazene Groups and Its Flame Retardant Mechanism on Epoxy Resin. *Polymer* **2011**, *52*, 5486–5493. [CrossRef]
48. Jian, R.; Wang, P.; Duan, W.; Wang, J.; Zheng, X.; Weng, J. Synthesis of a Novel P/N/S-Containing Flame Retardant and Its Application in Epoxy Resin: Thermal Property, Flame Retardance, and Pyrolysis Behavior. *Ind. Eng. Chem. Res.* **2016**, *55*, 11520–11527. [CrossRef]

Disclaimer/Publisher's Note: The statements, opinions and data contained in all publications are solely those of the individual author(s) and contributor(s) and not of MDPI and/or the editor(s). MDPI and/or the editor(s) disclaim responsibility for any injury to people or property resulting from any ideas, methods, instructions or products referred to in the content.

MOST WIEDZY Downloaded from mostwiedzy.pl